Charge-density and spin-density excitations in a two-dimensional electron gas with Rashba spin-orbit coupling

L. J. Xu and X. G. Wu
SKLSM, Institute of Semiconductors, Chinese Academy of Sciences, Beijing 100083, China
(Received 27 July 2006; revised manuscript received 6 September 2006; published 11 October 2006)

We study theoretically the charge-density and spin-density excitations in a two-dimensional electron gas in the presence of a perpendicular magnetic field and a Rashba type spin-orbit coupling. The dispersion and the corresponding intensity of excitations in the vicinity of cyclotron resonance frequency are calculated within the framework of random phase approximation. The dependence of excitation dispersion on various system parameters, i.e., the Rashba spin-orbit interaction strength, the electron density, the Zeeman spin splitting, and the Coulomb interaction strength is investigated.

DOI: 10.1103/PhysRevB.74.165315 PACS number(s): 73.21.Fg, 71.45.Gm, 71.70.Ej

I. INTRODUCTION

The emerging field of spintronics has generated an intense interest in the effect of spin-orbit interaction (SOI) in low-dimensional semiconductor structures.[1–3] The Rashba SOI[4] which arises from the inversion asymmetry of the confining potential is of particular interest as its strength may be varied in a controllable manner.[5–10] The dependence of Rashba SOI strength on the gate voltage has been studied experimentally by analyzing the beating pattern in the Shubnikov-de Haas (SdH) oscillations.[6–10]

The electron charge-density and spin-density excitations in a two-dimensional electron gas (2DEG) are collective excitations induced by the electron-electron (*e-e*) interaction.[11–18] In the presence of an external magnetic field, these excitations are called magnetoplasmons.[11] The energy and other characteristics of these excitations can be measured in optical experiments, for example, via infrared absorption[14] and inelastic light scattering measurement.[15–17]

There are extensive theoretical[11–13] and experimental investigations[17,18] on magnetoplasmons. However, in these theoretical works, SOI is usually ignored for simplicity and clarity. More recently, theoretical studies on collective excitations in a 2DEG, where the spin-orbit coupling was taken into account, were presented in the absence of an external magnetic field.[19–21] The intersubband spin-density excitation in a quantum well at zero magnetic field was studied within the local density-functional approach.[22]

In this paper, we wish to study theoretically the charge-density excitation (CDE) and spin-density excitation (SDE) in a 2DEG in the presence of a perpendicular magnetic field within the framework of random phase approximation (RPA). The Rashba SOI is taken into account explicitly. Complementary to previous theoretical works, we will study in detail the dependence of excitation dispersion on various system parameters, i.e., the Rashba spin-orbit interaction strength, the electron density, the Zeeman spin splitting, and the Coulomb interaction strength. In this work, the RPA is employed for simplicity. In the case of no spin-orbit coupling, RPA was found to give a correct description of the dispersion relation of charge density excitations in the long wavelength limit.[23]

The present paper is organized as follows: in Sec. II, the formulation and calculation scheme for charge-density and spin-density excitations are briefly reviewed. Although the standard RPA approach can be found in textbooks,[24] for clarity purposes, it is still necessary to introduce some notations which will be used throughout the paper. In Sec. III, we present our numerical results and discuss the underlying physics. Finally, a summary is presented in the last section.

II. FORMULATION AND CALCULATION

Let us consider a 2DEG in the xy plane with an external magnetic field $\mathbf{B}$ applied along the z direction. The vector potential is chosen as $\mathbf{A}=(0,Bx,0)$ in the Landau gauge. The interacting Hamiltonian can be written as

$$H=\sum_{\sigma\sigma'}\int d\mathbf{r}\psi^{\dagger}_{\sigma}(\mathbf{r})H^{0}_{\sigma\sigma'}\psi_{\sigma'}(\mathbf{r})$$
$$+\frac{1}{2}\sum_{\sigma\sigma'}\int d\mathbf{r}d\mathbf{r}'\psi^{\dagger}_{\sigma}(\mathbf{r})\psi^{\dagger}_{\sigma'}(\mathbf{r}')v(\mathbf{r}-\mathbf{r}')\psi_{\sigma'}(\mathbf{r}')\psi_{\sigma}(\mathbf{r}),$$

where $\psi_{\sigma}(\mathbf{r})$ is the field operator. H^0 is the single-electron Hamiltonian with Rashba SOI and it can be written as

$$H^{0}=\frac{1}{2m^{*}}\left(\mathbf{p}+\frac{e}{c}\mathbf{A}\right)^{2}+\frac{\alpha}{\hbar}\left[\vec{\sigma}\times\left(\mathbf{p}+\frac{e}{c}\mathbf{A}\right)\right]_{z}+\frac{1}{2}g^{*}\mu_{B}B\sigma_{z}$$

with m^* the effective mass of electrons, g^* the effective g-factor, μ_B the Bohr magneton, $\vec{\sigma}=(\sigma_x,\sigma_y,\sigma_z)$ the Pauli spin matrix, and α the Rashba SOI strength. The analytic solutions of the single-electron energy levels can be obtained and they are given by

$$E_0=(\hbar\omega_c-g\mu_B B)/2,$$

$$E_l^{\pm}=l\hbar\omega_c\mp\sqrt{E_0^2+2l\alpha^2/l_c^2},\quad l=1,2,\ldots,$$

with $\omega_c=eB/m^*c$ the cyclotron frequency, $l_c=\sqrt{\hbar c/eB}$ the magnetic length. This analytical solution has also been obtained by many others.

The charge-density correlation function χ_{ρ} and the spin-density correlation functions $\chi_{\sigma_z(\sigma_{\pm})}$ are defined for imaginary time τ as[11]

$$\chi_{\rho}(\mathbf{r},\mathbf{r}',\tau)=-\langle\rho(\mathbf{r},\tau)\rho(\mathbf{r}',0)\rangle,$$

 ©2006 The American Physical Society

$$\chi_{\sigma_z}(\mathbf{r},\mathbf{r}',\tau) = -\langle \sigma_z(\mathbf{r},\tau)\sigma_z(\mathbf{r}',0)\rangle,$$

$$\chi_{\sigma_\pm}(\mathbf{r},\mathbf{r}',\tau) = -\langle \sigma_\mp(\mathbf{r},\tau)\sigma_\pm(\mathbf{r}',0)\rangle,$$

where the charge-density operator ρ and the spin-density operator $\vec{\sigma}$ are defined as

$$\rho(\mathbf{r},\tau) = \sum_{\sigma_1} \psi^\dagger_{\sigma_1}(\mathbf{r},\tau)\psi_{\sigma_1}(\mathbf{r},\tau),$$

$$\vec{\sigma}(\mathbf{r},\tau) = \sum_{\sigma_1\sigma_2} \psi^\dagger_{\sigma_1}(\mathbf{r},\tau)\vec{\sigma}\psi_{\sigma_2}(\mathbf{r},\tau),$$

and $\sigma_\pm=(\sigma_x\pm i\sigma_y)/2$. Within the RPA, the correlation functions in the momentum and frequency space can be written as[24]

$$\chi_A(\mathbf{q},\omega) = P_A(\mathbf{q},\omega)[1 - v(q)D^0(\mathbf{q},\omega)/\hbar]^{-1}, \quad (1)$$

where the subscript A stands for ρ, σ_z, or $\sigma_\pm$. $v(q)=2\pi e^2/\epsilon_0 q$ with ϵ_0 the static dielectric constant. $D^0(\mathbf{q},\omega)=\Sigma_{\sigma_1\sigma_2}D^0_{\sigma_1\sigma_1,\sigma_2\sigma_2}(\mathbf{q},\omega)$, with $D^0_{\sigma_1\sigma_2,\sigma_3\sigma_4}(\mathbf{q},\omega)$ the density correlation function associated with $\psi^\dagger_{\sigma_1}\psi_{\sigma_2}$ and $\psi^\dagger_{\sigma_3}\psi_{\sigma_4}$ in the absence of e-e interaction. This corresponds to the bubble diagram in the language of the Feynman diagrammatic method.[24] This correlation function can be calculated in terms of the single-particle Green's functions

$$D^0_{\sigma_1\sigma_2,\sigma_3\sigma_4}(\mathbf{q},i\omega_n) = \frac{1}{\beta\hbar}\sum_{l_1l_2l_3l_4}\sum_{kk'}\langle l_1k'|e^{i\mathbf{q}\cdot\mathbf{r}}|l_2k\rangle \times\langle l_3k|e^{-i\mathbf{q}\cdot\mathbf{r}'}|l_4k'\rangle \times\sum_{i\omega_1} G^0_{l_2\sigma_2,l_3\sigma_3}(i\omega_1)G^0_{l_4\sigma_4,l_1\sigma_1}(i\omega_1 - i\omega_n),$$

where $|lk\rangle$ is the wave function for the single electron Hamiltonian without SOI, but $G^0_{l_1\sigma_1,l_2\sigma_2}(i\omega_n)$ is the single-particle Green's function with SOI included. Functions $P_A(\mathbf{q},\omega)$ can be obtained as follows:

$$P_\rho(\mathbf{q},\omega) = D^0(\mathbf{q},\omega),$$

$$P_{\sigma_z}(\mathbf{q},\omega) = D^0_{\uparrow\uparrow,\uparrow\uparrow} + D^0_{\downarrow\downarrow,\downarrow\downarrow} - 2D^0_{\uparrow\uparrow,\downarrow\downarrow} - 4\frac{v(q)}{\hbar}(D^0_{\uparrow\uparrow,\uparrow\uparrow}D^0_{\downarrow\downarrow,\downarrow\downarrow} - D^0_{\uparrow\uparrow,\downarrow\downarrow}D^0_{\downarrow\downarrow,\uparrow\uparrow}),$$

$$P_{\sigma_+}(\mathbf{q},\omega) = D^0_{\uparrow\downarrow,\downarrow\uparrow} - \frac{v(q)}{\hbar}\left(D^0_{\uparrow\downarrow,\downarrow\uparrow}D^0 - \sum_{\sigma_1\sigma_2} D^0_{\uparrow\downarrow,\sigma_1\sigma_1}D^0_{\sigma_2\sigma_2,\downarrow\uparrow}\right),$$

$$P_{\sigma_-}(\mathbf{q},\omega) = D^0_{\downarrow\uparrow,\uparrow\downarrow} - \frac{v(q)}{\hbar}\left(D^0_{\downarrow\uparrow,\uparrow\downarrow}D^0 - \sum_{\sigma_1\sigma_2} D^0_{\downarrow\uparrow,\sigma_1\sigma_1}D^0_{\sigma_2\sigma_2,\uparrow\downarrow}\right).$$

It can be shown that the correlation functions $\chi_A(\mathbf{q},\omega)$ are all independent of the direction of the wave vector $\mathbf{q}$.

The pole of the charge-density and spin-density response functions, $\omega_p(q)$, gives the excitation dispersion of the system. From Eq. (1), one sees that the dispersion relation of CDE and SDE is determined by the same equation

$$1 - \frac{v(q)}{\hbar}D^0(q,\omega_p) = 0.$$

At the pole ω_p, one may introduce the functions

$$S_A(q,\omega_p) = \left|\lim_{\omega\to\omega_p}(\omega-\omega_p)\chi_A(q,\omega)\right|.$$

It describes the relative intensities of the excitation. The stronger the function $S_A(q,\omega_p)$ is, the more easily the excitation spectrum can be observed at ω_p experimentally.

III. RESULTS AND DISCUSSIONS

In our numerical calculation, a set of dimensionless variables are adopted: energy levels are taken in the unit of the cyclotron resonance energy $\hbar\omega_c$ and length variables are taken in the unit of the magnetic length l_c. $\alpha^*=\alpha/(l_c\hbar\omega_c)$ denotes the Rashba SOI strength. $r_c=e^2/(\epsilon_0 l_c\hbar\omega_c)$, where ϵ_0 is a dielectric constant, describes Coulomb interaction strength, which is required to be a small value as RPA is a perturbation theory. We limit ourselves to $r_c<1$. The Zeeman spin splitting is described by $r_z=g^*\mu_B B/\hbar\omega_c = g^*m^*/m_e$ with m_e the free electron mass in vacuum. The value of electron density n_e is represented by the filling factor ν defined as $\nu=n_e/2\pi l_c^2$.

We will limit ourselves to the region $\nu>1$. In the region $\nu<1$, two-dimensional electrons may exhibit fractional quantum Hall effect[25] or Wigner crystal state.[26] In these cases, the electron correlation is very important,[27] however, the electron correlation is not included in RPA. In addition, the $k_BT \ll \hbar\omega_c$ limit is considered for simplicity. All parameters used in our numerical calculation are chosen such that they are in the experimentally accessible region.

First, let us examine the general feature of collective excitations. The collective excitation may be viewed as a coherent superposition of single-particle excitations with transition energies renormalized by the Coulomb interaction. When the spin-orbit coupling is taken into account, electrons are allowed to make transitions between Landau levels with different spins even in charge density excitations. In the case that the two lowest levels are fully or partially occupied, four excitation modes can be found in the vicinity of the cyclotron frequency, as shown in Fig. 1 for $r_c=0.3$, $r_z=-0.05$, $\nu=1.3$, and $\alpha^*=0.06$. For convenience, in Fig. 1, these modes are marked as ω_1, ω_2, ω_3, and ω_4 in turn from top to bottom, respectively. In the inset of Fig. 1, the lowest four energy levels and four single-particle transitions associated with the collective modes are shown schematically. The fully or partially occupied levels are shown by solid lines, and empty levels by dashed lines.

As the wave vector q increases, the mode ω_2 first increases rapidly until it meets mode ω_1. At this wave vector (about $ql_c=0.38$) modes ω_2 and ω_1 form an anticross. However, the splitting is so small that one can hardly see from the figure in its current scale. As q further increases, ω_2 becomes almost q independent until $ql_c=1.73$. After that ω_2 gradually decreases and approaches ω_c from above as q increases. Mode ω_1 first is almost q independent. When $ql_c>0.38$, it increases and reaches a maximum at $ql_c=0.95$. Around $ql_c=1.8$, mode ω_1 forms an anticross with mode ω_2. Beyond

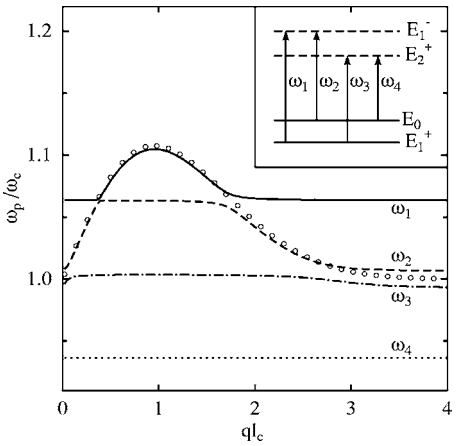

FIG. 1. Excitation spectra in the vicinity of the cyclotron frequency ω_c as a function of the wave vector ql_c. These four modes are marked as mode ω_1, ω_2, ω_3, and ω_4 in turn from top to bottom, which correspond to solid, dashed, dash-dotted, and dotted lines, respectively. Parameters used are Coulomb interaction strength $r_c=0.3$, Zeeman splitting $r_z=-0.05$, Rashba SOI strength $\alpha^*=0.06$, and the filling factor $\nu=1.3$. The dispersion curve in the absence of SOI is also plotted as open dots. The inset shows schematically the lowest four energy levels and four single-particle transitions associated with the collective modes. The fully or partially occupied levels are shown by solid lines, and empty levels by dashed lines.

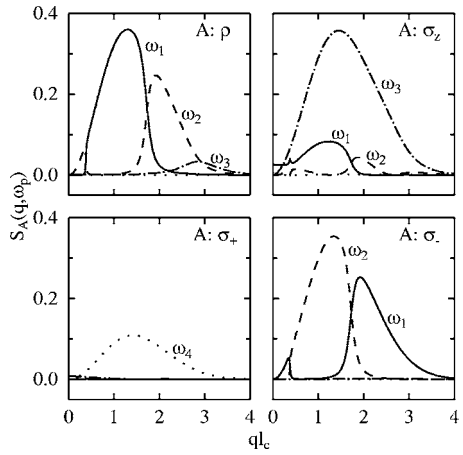

FIG. 2. CDE and SDE intensities $[S_A(q,\omega_p)]$ for each dispersion curve in Fig. 1 as a function of ql_c. In each panel, A stands for ρ, σ_z, σ_+, and σ_-, respectively.

this point, ω_1 is almost q independent. Unlike modes ω_1 and ω_2, mode ω_3 has only a slight dependence on the wave vector, and mode ω_4 is almost q independent.

Now let us study the behavior of the dispersion curves in the long wavelength limit. For simplicity and clarity, we will limit ourselves to the case that the filling factor ν is limited within 1 and 2. Without the loss of generality (g^* and α should not be too large), we may assume that two lowest levels are E_0 and E_1^+, respectively, and they are fully or partially occupied. ν_1 denotes the filling fraction of E_0, and ν_2 represents the occupation of E_1^+. Thus $\nu=\nu_1+\nu_2$. Omitting terms in the fifth and higher powers of ql_c, one can obtain analytic expressions for these four modes in the long wavelength limit:

$$\omega_1/\omega_c = (E_1^- - E_1^+)/\hbar\omega_c + \frac{r_c\nu_2\gamma_1^2}{4(1+\gamma_1^2)^2}(ql_c)^3,$$

$$\omega_2/\omega_c = (E_1^- - E_0)/\hbar\omega_c + \frac{r_c\nu_1}{2(1+\gamma_1^2)}ql_c,$$

$$\omega_3/\omega_c = (E_2^+ - E_1^+)/\hbar\omega_c + \frac{r_c\nu_2}{2(1+\gamma_1^2)(1+\gamma_2^2)}ql_c,$$

$$\omega_4/\omega_c = (E_2^+ - E_0)/\hbar\omega_c + \frac{r_c\nu_1\gamma_2^2}{8(1+\gamma_2^2)}(ql_c)^3.$$

Here $\gamma_n=(\sqrt{2}\alpha/l_c)/(E_0+\sqrt{E_0^2+2n\alpha^2/l_c^2})$. One observes that all four modes approach energy differences of single-particle energy levels, as $q\to 0$.

In the absence of SOI, it is well-known that the charge density excitation energy ω_p around ω_c always approaches ω_c as $q\to 0$, as required by Kohn's theorem.[28] This well-known theorem states that the cyclotron resonance frequency is not affected by the e-e interaction in a translational invariant system. When SOI is taken into account, Kohn's theorem is no longer applicable as the electric current contains a contribution from spin motion. However, our above $q\to 0$ result indicates that the Coulomb interaction still vanishes in the long wavelength limit. This is accidently because here only the direct Coulomb energy is considered due to the restrictions of the RPA method. We wish to point out that the differences of energy levels (single-particle transition energies), which give the excitation energies as $q\to 0$, are singly determined by the Zeeman spin splitting and Rashba SOI strength since energy levels are calculated within a single electron picture.

In Fig. 1, we also plot the dispersion curve $\omega(q)$ in the case of no SOI. It is plotted as open dots. As q increases, ω shifts away and back to ω_c, and this frequency shift $\Delta\omega=\omega-\omega_c$ is proportional to the e-e interaction strength.[11] In the case that SOI is taken into account, we may define frequency shifts $\Delta\omega_i$ $(i=1,2,3,4)$ as follows: $\Delta\omega_i=\omega_i-\omega_{i0}$, where $\hbar\omega_{i0}$ denotes the corresponding single particle transition energy. From Fig. 1, one sees that the sum of these frequency shifts $\Delta\omega'=\Sigma_i\Delta\omega_i$ as a function of ql_c follows a behavior similar to that $(\Delta\omega)$ in the absence of SOI. This observation suggests that one may view four modes shown in Fig. 1, in particular, the anticrossing behavior between the modes, as a consequence of coupling between mode $\omega(q)$ and four single-particle transitions ω_{i0} when they cross each other. This picture suggests that the existence of anticrosses requires a stronger e-e interaction for a fixed Zeeman splitting, or a smaller Zeeman splitting for a fixed e-e interaction strength. This will be discussed in more detail later.

To characterize collective excitations further, we study the intensities of these modes. In Fig. 2, functions $S_A(q,\omega_p)$ are plotted as a function of ql_c for these four modes. In each of four panels of Fig. 2, A stands for ρ, σ_z, σ_+, and σ_-, respectively. In each panel, we also mark a mode with a mode

identifier if this mode has a relatively strong intensity. The mode identifier marked has the same meaning as in Fig. 1. We wish to point out that by examining the strength, one may know the characteristic of a particular mode. For instance, if a mode has a relatively large value of S_ρ, then it should be easier to detect this mode via the charge density ρ response of the system. In this case, one may say that this mode is of CDE character.

Let us first examine the S_ρ panel of Fig. 2. For ql_c less than 0.38, the mode ω_2 has a larger intensity. When ql_c falls between 0.38 and 1.73, the mode ω_2 loses its intensity, while mode ω_1 becomes dominant. The intensity of mode ω_1 reaches a maximum at $ql_c=1.3$ and beyond this it falls monotonically. When ql_c becomes larger than 1.73, the mode ω_1 loses its intensity and the mode ω_2 regains intensity. The intensity of mode ω_2 reaches a maximum at $ql_c=1.92$ and then it falls as q further increases. The mode ω_3 only gains a weak intensity at large q. By comparing this panel with the behavior of dispersion curves shown in Fig. 1, one sees that when a mode exhibits a larger shift from the corresponding single-particle transition energy, then it usually has a larger intensity in S_ρ. Such a correlation is qualitatively true for modes ω_1 and ω_2, but is only partly true for the mode ω_2. The intensity of mode ω_2 shows two peaks while the dispersion curve of ω_2 only shows one broad peak.

Let us now turn to the S_{σ_z} panel of Fig. 2. One sees that except in a narrow small q region, mode ω_3 is the strongest one among four modes. It is interesting to note that ω_3 has no dramatic frequency shift in its dispersion curve as shown in Fig. 1. Modes ω_1 and ω_2 only show weak intensities in the regions where two modes have relatively large frequency shifts in their dispersion curves. Our numerical calculation shows (though not displayed in the figure) that mode ω_3 gets stronger, and modes ω_1 and ω_2 become weaker as the filling factor increases from $\nu=1$, a completely spin polarized state, to $\nu=2$, a spin nonpolarized state.

From the S_{σ_+} panel of Fig. 2, one sees that only mode ω_4 displays a relatively large intensity. From the S_{σ_-} panel in Fig. 2, one sees that the q dependence of mode ω_1 (mode ω_2) resembles the q dependence of mode ω_2 (mode ω_1) in the S_ρ panel. These two modes have strong intensities in the flat q regions of their dispersion curves. The S_{σ_-} intensity of modes ω_3 and ω_4 are very small.

Our above observations suggest that the mode ω_4 is primary of σ_+-SDE character, the mode ω_3 is primary of σ_z-SDE character, and modes ω_1 and ω_2 show either CDE or σ_--SDE character depending on the wave vector q. In the region where the mode ω_1 has CDE character, the mode ω_2 is of σ_--SDE character. When the mode ω_1 becomes σ_--SDE character, the mode ω_2 becomes CDE character.

It should be pointed out that in the above discussion for the general feature of CDE and SDE, the e-e interaction strength is assumed to be relatively strong. In the case that r_c is small or the absolute magnitude of r_z is large, the mode ω_2 will exhibit a relatively smooth dispersion curve, and there will be no anticross behavior between ω_1 and ω_2 modes. In this case, the mode ω_2 will exhibit a large S_ρ, and the mode ω_1 shows a large S_{σ_-}. Thus the mode ω_2 is primary of CDE character, and the mode ω_1 is primary of σ_--SDE character.

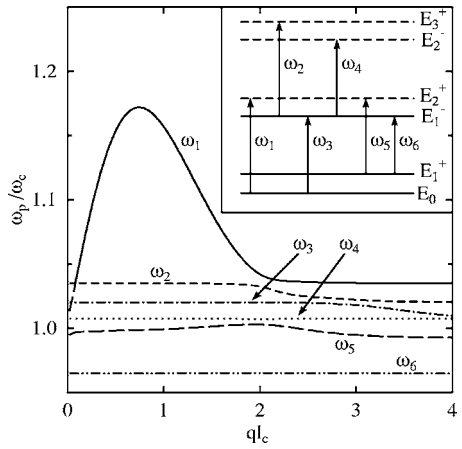

FIG. 3. Excitation spectra near ω_c as a function of ql_c for $r_c=0.3$, $r_z=0.05$, $\alpha^*=0.06$, and $\nu=2.7$. The modes are marked as ω_1, ω_2, ω_3, ω_4, ω_5, and ω_6 in turn from top to bottom, respectively. The inset shows schematically the lowest six energy levels and six single-particle transitions associated with the collective modes. The fully or partially occupied levels are shown by solid lines, and empty levels by dashed lines.

Next let us study the general feature of collective excitations when the electron density is higher. In Fig. 3, the dispersion curves of excitation modes around ω_c are shown for the case $\nu=2.7$ and $r_z=0.05$. The corresponding intensities of these excitation modes are shown in Fig. 4. For this filling factor, the lowest three energy levels are occupied, and there are six modes around ω_c. In Fig. 3, these modes are marked as ω_1 to ω_6 in turn from top to bottom. The inset of Fig. 3 shows schematically the lowest six energy levels and six single-particle transitions associated with the collective modes. The fully or partially occupied levels are shown by solid lines, and empty levels by dashed lines. Among the top three modes, anticrosses appear between mode ω_2 and ω_3 at $ql_c=0.04$ and 2.9, and between mode ω_1 and ω_2 at $ql_c=0.08$ and 2.04. The mode ω_1 develops a large peak and reaches maximum at $ql_c=0.74$. Other modes show small wave vector dependence.

The top three modes show the CDE characteristics in the regions where they have large frequency shifts in their dis-

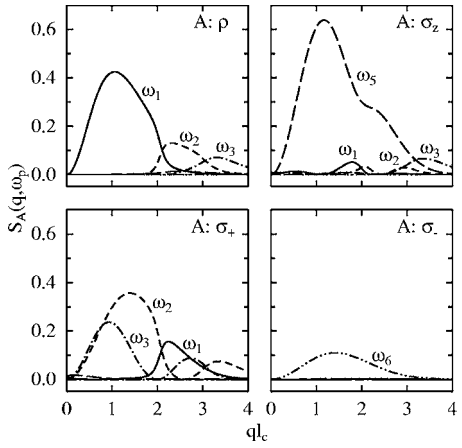

FIG. 4. CDE and SDE intensities for each dispersion curve in Fig. 3.

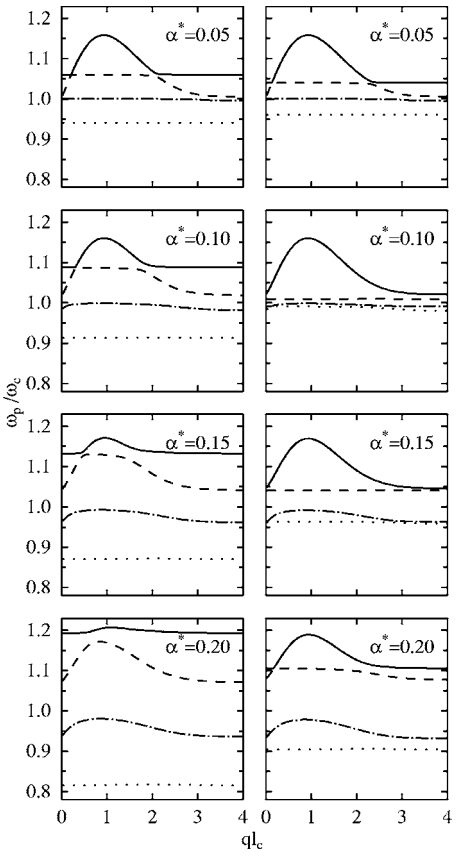

FIG. 5. Excitation spectra in the vicinity of ω_c as a function of ql_c for $\alpha^*=0.05$, 0.1, 0.15, and 0.2 with $r_c=0.3$ and $\nu=2.0$. Left panels are for $r_z=-0.05$, and right panels are for $r_z=0.05$.

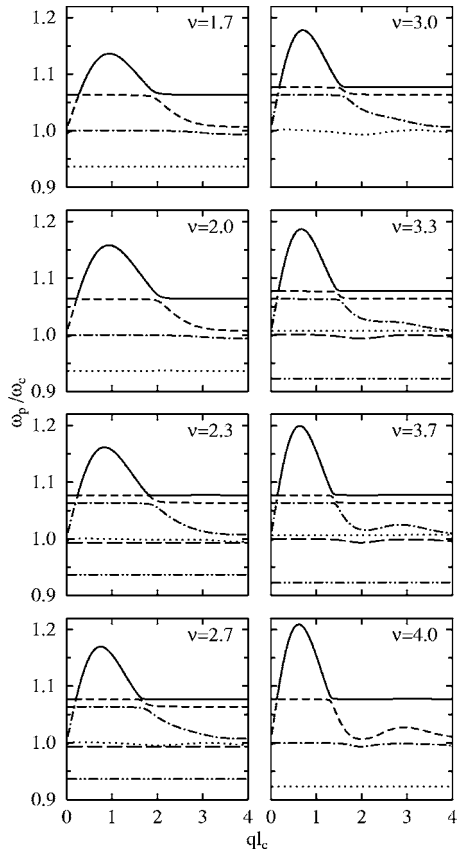

FIG. 6. Excitation spectra around ω_c as a function of ql_c for various values of the filling factor ν. $r_c=0.3$, $r_z=-0.05$, and $\alpha^*=0.06$.

persion curves. The mode ω_5 is of σ_z-SDE character. The S_{σ_+}-SDE intensity is strong for the top three modes in regions where their dispersion curves are almost q independent, and the lowest mode is of S_{σ_-}-SDE character.

It is interesting to note that the lowest mode is primarily of σ_--SDE character in Fig. 4, while it is primarily of σ_+-SDE character in Fig. 2. By examining Figs. 1 and 3, one finds that the lowest excitation mode is almost q independent, and its excitation energy is close to the single particle transition energy. In Fig. 1, $r_z=-0.05$, the lowest excitation mode is related to the single particle transition energy $E_2^+ - E_0$, and the mode is of S_{σ_+}-SDE character. In Fig. 3, $r_z=0.05$, the excitation energy of the lowest mode is close to $E_1^- - E_1^+$, and the mode is of S_{σ_-}-SDE character. From this observation, one may conclude that a mode showing a σ_+ or σ_--SDE character depends on the relative spin orientations of participating single particle transition energy levels, as the excitation may be viewed as a coherent superposition of the single particle excitation with e-e interaction renormalization.

Having in mind the general picture of excitation spectra in the presence of Rashba SOI, we now turn to discuss the influences of various system parameters. First, the effect of Rashba SOI strength on excitation spectra will be investigated. In Fig. 5, dispersion curves of excitation modes around ω_c are plotted for $\alpha^*=0.05, 0.1, 0.15, 0.2$, $r_c=0.03$, and $\nu=2.0$. Left panels are for $r_z=-0.05$, and right panels are for $r_z=0.05$. As in Fig. 1, these modes are named ω_1, ω_2, ω_3, and ω_4 in turn from top to bottom.

Let us discuss the case of $r_z=-0.05$ first (see left panels of Fig. 5). The energy differences between these modes increase as α^* increases. The q distance between two anticross points due to the coupling among the top two modes gradually becomes smaller, as α^* increases starting from $\alpha^*=0.05$. When $\alpha^*=0.2$, the anticrossing behavior no longer exists. Additionally, the increase of α^* induces a more pronounced wave vector dependence for the mode ω_3.

In the case of $r_z=0.05$, however, the excitation modes around ω_c vary in a different way (see right panels of Fig. 5) compared to the case of $r_z=-0.05$. At $\alpha^*=0.1$, the mode ω_1 is a smooth curve, and no anticross is found between the top two modes. Instead, two anticrosses emerge between the lowest two modes at $ql_c=0.1$ and 2.3. At $\alpha^*=0.15$, both modes ω_1 and ω_3 are smooth curves. As α^* further increases, the anticross behavior occurs between the top two modes again.

Next, we turn to discuss the effects of the filling factor on excitations spectra. Figure 6 shows dispersion curves around ω_c for various values of filling factor ν. The excitation energy in the $q\to 0$ limit is equal to the single electron transition energy, thus the frequency of each mode at long wavelength limit or when $ql_c \gg 1$ is independent of filling factor ν. The number of modes around ω_c depends on the filling factor. When $1<\nu<2$, there are four modes. When $2<\nu<4$, there are six modes. At $\nu=2$ and $\nu=4$ there are four modes.

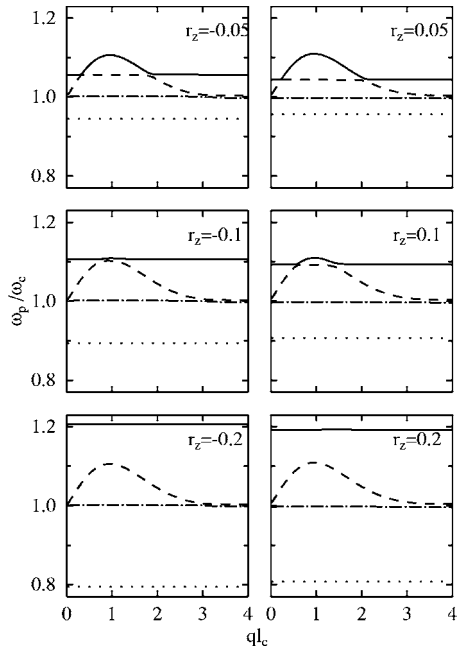

FIG. 7. Excitation spectra around ω_c as a function of ql_c for a various values of Zeeman spin splitting r_z. r_c=0.3, α^*=0.04, and ν=1.3.

The number of modes can be estimated by counting all possible single particle transitions. This simple estimation should work when the Rashba SOI is weak and the Zeeman splitting is not too large. From Fig. 6, one sees that the anticross behaviors occur between the top two modes or top three modes depending on the filling factor. The wave vectors where these anticrosses occur depend on the filling factor. However, the splitting size of anticross seems to vary little as filling factor changes. Similar to the discussion about Fig. 1, one observes that the sum of frequency shifts of these modes closely follows the behavior of dispersion curve in the case of no SOI as Rashba SOI strength is taken as a small value here.

The effect of Zeeman splitting on the excitation is illustrated in Fig. 7. As r_z increases, the top mode moves to higher energy, the bottom mode moves to lower energy, and two modes in the middle show no significant change except in the region of anticrosses. One sees that the overall dependence of dispersion curves on the Zeeman spin splitting is quite similar between $r_z<0$ (left panels) and $r_z>0$ (right panels). As we discussed before, one may consider the four modes shown in Fig. 7 resulted from the coupling between four single particle transitions and the charge density mode without Rashba SOI. Similarly, one may use this qualitative picture to understand the influence of *e-e* interaction on the collective excitations. In Fig. 8, dispersion curves around ω_c are shown for various values of *e-e* interaction strength. The increase of r_c induces a frequency shift of top mode, and the positions of the two anticrosses become wider as r_c increases.

Next, the dispersion curves of low-lying excitations are shown in Fig. 9. Two cases are shown: r_z=−0.05 and ν=1.3 in panels (a) and (b), r_z=0.05 and ν=2.7 in panels (c) and (d). The corresponding excitation intensity is shown in

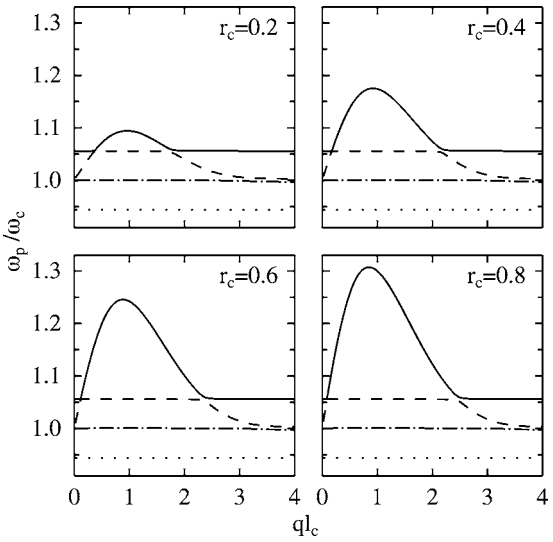

FIG. 8. Excitation spectra around ω_c as a function of ql_c for various values of Coulomb interaction strength r_c. r_z=−0.05, α^*=0.04, and ν=1.7.

panels (b) and (d), respectively. The other variables are r_c=0.3 and α^*=0.06. One finds that the dispersion curves have negligible frequency shift when the filling factor or Zeeman spin splitting varies. However, the mode shown in panel (a) is of σ_--SDE character as shown in panel (b). The mode shown in panel (c) is of σ_+-SDE character as shown in panel (d). This is because low-lying modes originate from single particle energy level transitions with different spin orientations, as the Zeeman spin splitting takes opposite value in panels (a) and (c).

Finally, we wish to point out that our calculation is based on the RPA for simplicity. In this approximation, one neglects the exchange and correlation correction to the electron self-energy. The dispersion curve becomes unreliable for very large wave vectors. In the case of no spin-orbit interaction, the electron density correlation function and magnetoplasmon modes were investigated beyond RPA for a two-dimensional electron gas.[11] It shows that the dispersion will change slightly in the long wavelength limit. One also obtains the correct dispersion for large wave vectors. It is possible to extend the present calculation along the same line. In

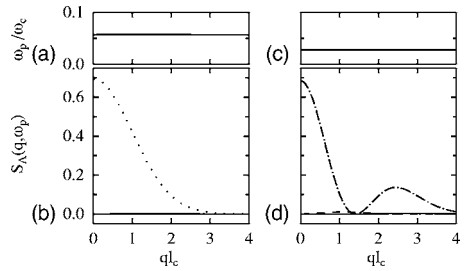

FIG. 9. Low-lying excitation spectrum and its corresponding intensities as a function of ql_c for r_z=−0.05 and ν=1.3 in (a) and (b), and for r_z=0.05 and ν=2.7 in (c) and (d). In panels (b) and (d), functions S_ρ, S_{σ_z}, S_{σ_+}, and S_{σ_-} correspond to solid, dashed, dash-dotted, and dotted lines, respectively. Other parameters used are r_c=0.3 and α^*=0.06.

doing so, similar to the case of no spin-orbit coupling, the dispersion curve should be modified for large wave vectors. Moreover, one would expect that the collective mode associated with transitions between different spins will be more strongly modified by the electron-electron interaction. Our preliminary investigation indicates that the collective mode below the cyclotron resonance may display a mode softening behavior driven by the Rashba spin-orbit interaction strength. This behavior is not present within the RPA approach as shown in Fig. 9. In our numerical calculations, the dimensionless parameter r_c ranges from 0.2 to 0.8. For a quantum well made of InAs (the effective mass is $m^*=0.023m_e$ and the dielectric constant is $\varepsilon_0=14.5$), this corresponds to a magnetic field between 14.8 and 0.9 T, experimentally accessible in a laboratory. The parameter α^* has been chosen between 0.05 and 0.2, and this corresponds to α ranging from 16.5 to 66.3 meV nm. This is largely within the experimentally accessible range.[10] We wish that our theoretical study will inspire some experimental investigations.

IV. SUMMARY

In summary, we have studied charge- and spin-density excitations in a two-dimensional electron gas in the presence of a perpendicular magnetic field with the Rashba spin-orbit interaction taken into account. Electrons are allowed to make transitions between energy levels with different spins, and four or six collective modes in the vicinity of the cyclotron resonance frequency can be found when more than one energy level is occupied. It is found that each mode approaches the single-electron transition energy in the long wavelength limit. The intensity of these modes are analyzed, and it is found that some modes may have either CDE or SDE character and their character may vary depending on the wave vector. It is also found that the dispersion curves and the corresponding intensities may be substantially affected by the strength of electron-electron interaction, the Zeeman spin splitting, the Rashba spin-orbit coupling, and system occupations.

ACKNOWLEDGMENT

This work was partly supported by the NSF of China.

[1] S. Datta and B. Das, Appl. Phys. Lett. **56**, 665 (1990).
[2] T. Koga, J. Nitta, H. Takayanagi, and S. Datta, Phys. Rev. Lett. **88**, 126601 (2002).
[3] Y. K. Kato, R. C. Myers, A. C. Gossard, and D. D. Awschalom, Science **306**, 1910 (2004).
[4] Yu. A. Bychkov and E. I. Rashba, Pis'ma Zh. Eksp. Teor. Fiz. **39**, 66 (1984) [JETP Lett. **39**, 78 (1984)]; J. Phys. C **17**, 6039 (1984).
[5] J. Luo, H. Munekata, F. F. Fang, and P. J. Stiles, Phys. Rev. B **38**, 10142 (1988); **41**, 7685 (1990).
[6] G. Engels, J. Lange, Th. Schäpers, and H. Lüth, Phys. Rev. B **55**, R1958 (1997).
[7] J. Nitta, T. Akazaki, H. Takayanagi, and T. Enoki, Phys. Rev. Lett. **78**, 1335 (1997).
[8] J. P. Heida, B. J. van Wees, J. J. Kuipers, T. M. Klapwijk, and G. Borghs, Phys. Rev. B **57**, 11911 (1998).
[9] C. M. Hu, J. Nitta, T. Akazaki, H. Takayanagai, J. Osaka, P. Pfeffer, and W. Zawadzki, Phys. Rev. B **60**, 7736 (1999).
[10] D. Grundler, Phys. Rev. Lett. **84**, 6074 (2000).
[11] C. Kallin and B. I. Halperin, Phys. Rev. B **30**, 5655 (1984).
[12] A. H. MacDonald, J. Phys. C **18**, 1003 (1985).
[13] H. C. A. Oji and A. H. MacDonald, Phys. Rev. B **33**, 3810 (1986).
[14] E. Batke, D. Heitmann, and C. W. Tu, Phys. Rev. B **34**, 6951 (1986).
[15] A. Pinczuk, J. P. Valladares, D. Heiman, A. C. Gossard, J. H. English, C. W. Tu, L. Pfeiffer, and K. West, Phys. Rev. Lett. **61**, 2701 (1988).
[16] A. Pinczuk, S. Schmitt-Rink, G. Danan, J. P. Valladares, L. N. Pfeiffer, and K. W. West, Phys. Rev. Lett. **63**, 1633 (1989).
[17] M. A. Eriksson, A. Pinczuk, B. S. Dennis, S. H. Simon, L. N. Pfeiffer, and K. W. West, Phys. Rev. Lett. **82**, 2163 (1999).
[18] G. Brozak, B. V. Shanabrook, D. Gammon, and D. S. Katzer, Phys. Rev. B **47**, 9981 (1993).
[19] G. H. Chen and M. E. Raikh, Phys. Rev. B **59**, 5090 (1999).
[20] W. Xu, Appl. Phys. Lett. **82**, 724 (2003).
[21] X. F. Wang, Phys. Rev. B **72**, 085317 (2005).
[22] C. A. Ullrich and M. E. Flatté, Phys. Rev. B **66**, 205305 (2002); **68**, 235310 (2003).
[23] E. Batke, D. Heitmann, J. P. Kotthaus, and K. Ploog, Phys. Rev. Lett. **54**, 2367 (1985).
[24] G. D. Mahan, *Many-Particle Physics* (Plenum, New York, 1990).
[25] R. B. Laughlin, Phys. Rev. Lett. **50**, 1395 (1983).
[26] E. Wigner, Phys. Rev. **46**, 1002 (1934).
[27] G. Murthy and R. Shankar, Rev. Mod. Phys. **75**, 1101 (2003).
[28] W. Kohn, Phys. Rev. **123**, 1242 (1961).